Date 25 november 2004
Author Evert Jan Foeth
Address Delft University of Technology
Ship Hydromechanics Laboratory
Mekelweg 2, 26282 CD Delft
Phone: +31 15 2786873

TU**Delft**

Delft University of Technology

Exploratory Experiments to Determine Flow and Structure Borne Noise of Erosive Cavity Implosions

by

Evert Jan Foeth and Gert Kuiper

Report No. 1413-P **2004**

ASME
SETTING THE STANDARD
1880 — 2005

HT/FED 2004

2004 ASME Heat Transfer/Fluids Engineering Summer Conference

July 11–15, 2004
Charlotte, North Carolina USA

Table of Contents

About HT/FED2004

About This Disc

Author Index

AIChE

**2004 ASME HEAT TRANSFER/FLUIDS ENGINEERING
SUMMER CONFERENCE**

July 11-15, 2004 • Charlotte, North Carolina USA

TABLE OF CONTENTS

ABOUT HTFED2004

LIST OF TOPICS

Fundamental Research and Measurements

Energy Systems

Industrial Processes, Equipment, and Machinery

Computational Fluid Dynamics and Heat Transfer

Transport Phenomena in Multiphase Flows

Aerospace and Vehicular Flows and Heat Transfer

Transport Phenomena in Manufacturing and Materials

Micro/Nano Fluid Dynamics and Heat Transfer Processing

Heat and Mass Transfer in Biotechnology

Transport Phenomena in Process Industry

Free Surface Flows and Environmental Heat Transfer

General Papers

Special Lectures

• • Transport Phenomena in Multi-Phase Flows • •

CAVITATION AND INDUSTRIAL APPLICATIONS OF MULTIPHASE FLOWS

FLOW AND HEAT TRANSFER IN MULTIPHASE SYSTEMS

HT-FED2004-56270
Mass Transfer During Fluid Sphere Dissolution in an Alternating Electric Field
Tov Elperin, Andrew Fominykh, and Zakhar Orenbakh

HT-FED2004-56298
Mutation Growth of Ice Crystal During Frost Formation
Z. M. Li and X. F. Peng

HT-FED2004-56337
A Two-Temperature Model for Solid/Liquid Phase Change in Metal Foams
Shankar Krishnan, Jayathi Y. Murthy, and Suresh V. Garimella

HT-FED2004-56389
Particle Velocity Measurements to Improve Erosion Prediction
Matthew J. M. J. Sampson, Siamack A. Shirazi, and Brenton S. McLaury

HT-FED2004-56403
Effect of Fluid Loading on the Performance of Wicked Heat Pipes
R. Kempers, A. Robinson, C. Ching, and D. Ewing

HT-FED2004-56410
Temperature Distribution in a Diode End-Pumped Solid State Laser Slab Subject to Two-Phase Spray Cooling
Brian E. Tews, Gregory S. Cole, R. Paul Roth, and Kunal Mitra

HT-FED2004-56445
Cross-Sectional Imaging of the Liquid Film in Horizontal Two-Phase Annular Flow
Daniel J. Rodriguez and Timothy A. Shedd

HT-FED2004-56584
Three Dimensional Velocity Measurements in an Automotive-Sized Evaporator Using Particle Image Velocimetry
Steven P. O'Halloran, B. Terry Beck, Mohammad H. Hosni, and Steven J. Eckels

HT-FED2004-56614
Heat Transfer Measurements and Correlations for Air-Water Two-Phase Slug Flow in a Horizontal Pipe
Afshin J. Ghajar, Kapil Malhotra, Jae-yong Kim, and Steve A. Trimble

HT-FED2004-56618
Rayleigh-Taylor Instability Mechanism on Sonoluminescing Bubble
Sarng Woo Karng, Yoon Pyo Lee, and Ho-Young Kwak

HT-FED2004-56703
Experimental Investigation on the Correlations of the Holdup and the Frictional Pressure Drop of Gas-Liquid Two-Phase Flow in a Flat Capillary Rectangular Channel
Hideo Ide and Tohru Fukano

FUNDAMENTALS AND APPLICATIONS OF BOILING

HT-FED2004-56056
Critical Heat Flux for Downward Facing Boiling on a Coated Hemispherical Surface
J. Yang, M. B. Dizon, F. B. Cheung, J. L. Rempe, K. Y. Suh, and S. B. Kim

HT-FED2004-56169
Time and Space Resolved Wall Temperature Measurements During Nucleate Boiling With Constant Heat Flux Boundary Conditions
Jerry G. Myers, Sam W. Hussey, Glenda F. Yee, Vamsee K. Yerramilli, and Jungho Kim

HT-FED2004-56179
Effect of Impact Velocity and Substrate Temperature on Boiling of Water Droplets Impinging on a Hot Stainless Steel Surface
N. Z. Mehdizadeh and S. Chandra

HT-FED2004-56183
Experimental Investigation of Heat Transfer Characteristics of Inkjet Assisted Spray Cooling
Ratnesh K. Sharma, Cullen E. Bash, and Chandrakant D. Patel

HT-FED2004-56240
Numerical Investigation on the Conjugate Heat Transfer in Double-Pipe Heat Exchangers With Propane Flow Boiling
Xuelei Chen, Mauricio A. Sánchez, and William H. Sutton

HT-FED2004-56301
CHF in Vertical Round Tubes With Uniform Heat Flux
W. Jaewoo Shim and Ji-Su Lee

HT-FED2004-56442
Detailed Characterization of Two-Phase Annular Flow in a Horizontal Tube
DuWayne Schubring and Timothy A. Shedd

HT-FED2004-56465
A Mechanistic Model for Predicting Heat and Mass Transfer in Vertical Two-Phase Flow
Siamack A. Shirazi, Ebrahim Al-Adsani, John R. Shadley, and Edmund F. Rybicki

HT-FED2004-56519
Correlation of Surface and Interfacial Energies on Enhanced Pool Boiling Heat Transfer
Elva Meléndez and René Reyes

HT-FED2004-56554
Effect of Flow Orientation on Critical Heat Flux in Subcooled Flow Boiling
Jason B. Bower and James F. Klausner

HT-FED2004-56555
Cryogenic Two-Phase Flow During Chilldown
Christopher Velat, Jeliffe Jackson, James F. Klausner, and Renwei Mei

HT-FED2004-56678
Numerical Study of an Evaporating Meniscus on a Moving Heated Surface
Abhijit Mukherjee and Satish G. Kandlikar

NUMERICAL METHODS FOR MULTIPHASE FLOW

HT-FED2004-56079
Parallelized Domain Decomposition Techniques for Multiphase Flow
Eray Uzgoren, Wei Shyy, and Marc Garbey

HT-FED2004-56083
Steady State Modeling of a Rotating Heat Pipe With a Composite Wick Structure
T. A. Jankowski, J. A. Waynert, F. C. Prenger, and A. Razani

HT-FED2004-56114
A Viscoelastic VOF-PROST Code for the Study of Drop Deformation
Y. Renardy, T. Chinyoka, D. B. Khismatullin, and J. Li

HT-FED2004-56136
N-Phase Interface Tracking Method Based on Prime Enumeration of Microcells
Mary Ann D. Clarke and Christopher J. Freitas

HT-FED2004-56142
Particle/CIP Hybrid Method for Predicting Motions of Micro and Macro Free Surfaces
Eiji Ishii, Toru Ishikawa, and Yoshiyuki Tanabe

HT-FED2004-56236
Accurate Time-Dependent Computations and Reduced-Order Modeling for Multiphase Flows
Yogen Utturkar, Siddharth Thakur, and Wei Shyy

HT-FED2004-56268
Computations of Boiling Flows
Grétar Tryggvason and Asghar Esmaeeli

HT-FED2004-56276
Parallel CFD-DEM for Fluid-Particle Systems
Xiang Zhao, Jun Wang, and Sijun Zhang

HT-FED2004-56315
Simulation of the Critical Flashing Flow With the Transient 1D Two-Fluid Model
Janez Gale and Iztok Tiselj

HT-FED2004-56377
Computational Analyses of Cavitating Control Elements in Cryogenic Environments
V. Ahuja, A. Hosangadi, and J. Shipman

HT-FED2004-56665
Multiphase Particle-in-Cell Simulations of Dense-Phase Flows in Cyclone Separators
Dale Snider, Ken Williams, and Robert A. Johnson

HT-FED2004-56726
Evaluation of the Parallel Parent and Daughter Classes Technique (PPDC) for Solving Population Balance Equations by Discretization: Aggregation and Breakage
Stefano Bove, Tron Solberg, and Bjørn H. Hjertager

TRANSPORT PHENOMENA IN GAS-SOLID-LIQUID THREE-PHASE FLOW SYSTEMS

HT-FED2004-56013
Modelling of Slurry-Handling Piping Element Under Interference Conditions
Prem Chand, K. Govinda Rajulu, and Y. Krishna Reddy

HT-FED2004-56220
Gas Holdup in a Cocurrent Air-Water-Fiber Bubble Column
Chengzhi Tang and Theodore J. Heindel

HT-FED2004-56222
Effect of Gas Distributor on Gas Holdup in Fiber Suspensions
Xuefeng Su and Theodore J. Heindel

HT-FED2004-56227
Artificial Neural Network-Based Flow Regime Classification Techniques for Gas-Liquid-Fiber Three-Phase Flows
T. Xie and S. M. Ghiaasiaan

HT-FED2004-56480
Study on Particle Response to Local Fluid Velocity in a Gas Particle Turbulent Flow
Bing Wang, Hui-qiang Zhang, and Xi-lin Wang

HT-FED2004-56686
Radiation Heat Transfer and Soot Thermophoresis in Laminar Tube Flow
M. K. Akbar and S. M. Ghiaasiaan

HT-FED2004-56844
Turbulent Multi-Phase Flow Interactions Through Grid Turbulence Measured by Particle Image Velocimetry
Michael R. Brady, D. Telionis, and Pavlos P. Vlachos

EXPLORATORY EXPERIMENTS TO DETERMINE FLOW AND STRUCTURE BORNE NOISE OF EROSIVE CAVITY IMPLOSIONS

Evert-Jan Foeth
Technical University of Delft

Gert Kuiper
Maritime Research Institute of the Netherlands

ABSTRACT

In two exploratory setups, a high-frequency pressure transducer has been used to determine both the flow and the structure borne noise above 200 kHz. In the first set of tests the impact noise due to a single bubble is investigated in order to gain insight in the acoustic signals emitted by an imploding bubble. A quantitative analysis of the signals indicates a short and clear acoustic signal in the fluid and a long chiming signal in the structure.

In the second set of tests the noise signal emitted by sheet cavitation implosion on a hydrofoil is acquired. The convoluted signals of individual bubbles can be identified both in the fluid and in the structure. Analyses of the signals by examining the peak distribution for sheet cavitation indicates a relation with the cavitation index and suggest that fluid and structure borne noise are not per se linked. Acoustic signals correlate well with visual observation.

INTRODUCTION

Predicting cavitation erosion on ship propellers is still a problem that remains unresolved. Although the latest numerical predictions have carried the cavitation model from simple 2D potential codes to more complex 3D Euler or even RANS solvers, the use of these programs remains time-consuming and the results insufficiently reliable. Predicting the cavitation pattern is a difficult task in itself, predicting the erosive characteristics even more so. The most frequently used technique for determining the erosive behavior of cavitation is a visual assessment from observations of a model test.

Qualitative techniques are soft metal methods and paint tests. The weight loss and location of the erosion can be used as a good erosion indicator. However, these tests are expensive, considering the need for more models and time for a test run (very soft aluminum requires 1 to 10 hours)[1]. Mass loss needs to be measured on a regular basis; this is prohibitively time-consuming for commercial tests where 30 minutes is considered an upper time limit. Paint tests, as used by the Swedish model basin SSPA, offer a more practical approach; the model propeller is coated with stencil ink and tested in a water tunnel for half an hour (an acceptable time limit). The results often correlate well with erosion patterns found on full scale. However, calibration of the observation and repeatability are uncertain and this technique does not predict the erosion severity.

Erosion occurs through the impact of imploding cavities on the propeller surface. This necessarily leaves an acoustic footprint both in the material as in the fluid. Therefore, is it possible to listen to erosion taking place? The goal of the setup described here is to study the feasibility of detecting cavitation erosion by means of its acoustic signature in the fluid as well as the structure born noise by cavitation impact on a test subject. Cavitation noise generated by implosion of bubbles is a high frequency signal, above a few tens of kilohertz up to a few megahertz[2]. As such, it is easily identifiable from flow noise or other noise sources. The source of this noise is cavitating bubbles imploding in the flow. The presence of a nearby surface alters the collapse mechanism of the bubble resulting in a change in the acoustic signature. The impact of a collapsing bubble on a surface should be audible in the test subject as well, as part of the energy is transferred to the material.

If successful, the location will remain an unknown so this so-called impact method cannot be used as the sole technique for erosion detection. However, the impact method can be used in concert with visual cavitation observations giving an additional tool to identify the erosivity of the implosion.

NOMENCLATURE

p	Pressure
p_v	Vapor Pressure
R	Bubble radius
s	Distance bubble-hydrophone
t_c	Bubble half collapse time
V	Flow velocity
γ	Dimensionless distance bubble-wall
ρ	Density
σ	Cavitation number

EXPERIMENTAL SETUP: SINGLE BUBBLE IMPACT

The test setup uses a spark probe as a bubble generator in polyacrylate basin of limited dimensions, see fig. 1. The polyacrylate is acoustically transparent so that wall reflections are reduced. A spark of 10 kV, discharging in period of 10 μs between 2 electrodes 0,1 mm apart, creates a bubble of arbitrary size. The acoustic transducers used are PCB Piezotronic 138M103 transducers with a resonance frequency of >2 MHz and a rise time of 0,5 μs. The transducer in the flow is placed in a polyacrylate container filled with silicon oil to prevent the formation of air-bubbles directly on the sensor. A similar sensor is placed in a chamber in the top of a bronze rod functioning as the impact object, also filled with silicon oil. The signal is acquired using a National Instruments 5911 DAQ capable of a maximum sampling rate of 100 MHz. The signals are acquired at 12,5 MHz both for the fluid as for the structure sensors(In hindsight 5 MHz will suffice) and processed

with a 200 kHz high pass filter. This will remove any spurious signals due to the remaining charge in the spark generator.

Images are acquired using a Kodak Ultima 40K high-speed digital camera, able to record a 64 by 64 pixel area at 40,500 frames per second. About 20 ms are needed from bubble initiation until its first collapse, resulting into roughly 20 images for the entire process. Because in the final collapse phase the bubble radius reduces exponentially, the actual collapse cannot be captured with this relatively low recording speed. Phillip & Lauterborn reported that even 20 million frames per second are insufficient to resolve the passage of the bubble through its minimum volume, albeit at a level of detail far beyond the need of this experiment[3].

The maximum radius of the bubble generated with the spark is varying in magnitude. Misfires are often encountered depending on probe surface and water quality. In case of a misfire, the generation of hydrogen gas can be observed (simple electrolysis). As a result, formation of small gas bubbles beneath the impact rod is nearly unavoidable. The signal form the two sensors are recorded separately, no direct correlation is measured for a single bubble event.
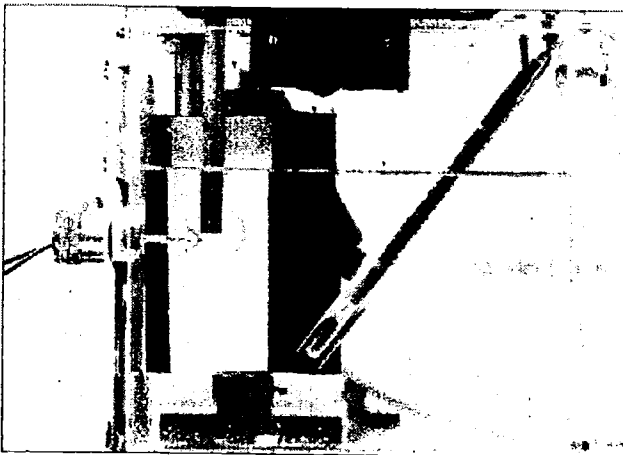

Figure 1 Experimental setup single bubble impact

A small delay is observed between the generation of the spark and the signal in the fluid of the rapidly growing bubble. The delay is the traveling time of the pressure wave at the speed of sound from the impact to the pressure transducer:

$$\Delta t = \frac{C_\infty}{s} \tag{1}$$

with $C \cong 1,5 \cdot 10^3$ m/s. The distance to the transducer is acoustically estimated at 83±1 mm with an average delay of 55,7 µs. This value agrees well with a (crude) measurement by ruler. However, the distance to the hydrophone is not relevant; no attempt has been made to calibrate the signals of the transducers, as the first stage of the setup is to determine the presence of a qualitative relationship.

EXPERIMENTAL SETUP: SHEET IMPACT

The second series of tests are performed in the High Speed Cavitation Tunnel at MARIN, Wageningen, the Netherlands. The water tunnel is approximately 2 meters long and is fitted with a 40 by 80 mm test section where a simple 2D NACA0018-45 foil is placed. The foil

can be freely rotated long its mid chord axis. Leading edge roughness is applied for turbulence tripping.

The same PCB 138M103 transducers are used but placed in an encapsulated differential pre-amplifier to suppress the interference from the tunnel's main drive. The structure sensor is placed in the foil, mid span, in a small hole drilled from the foil's support in the tunnel window. The fluid sensor is placed in a recess in the top window. Both chambers are filled with silicon oil. To set the conditions, the cavitation number at the center of the test section is defined as

$$\sigma = \frac{p - p_v}{\frac{1}{2}\rho V^2} \tag{2}$$

The velocity of the flow in the water tunnel is determined from Bernoulli using the pressure drop over the contraction upstream of the test section without calibration by e.g. LDV. The pressures are measured using mercury manometers for pressure up to and slightly over 1 bar, higher values require the use of a dial manometer. This dial manometer is known to be inaccurate, but is calibrated up to 1 bar with the mercury manometer. This calibration is extrapolated to higher pressures. An oscillation in the tunnel's main drive rpm results in a variation of the operation condition. In combination with the factors named above, a 5% deviation in σ is to be expected.

An over pressure is necessary in the test section to obtain the required cavitation number. Leakage in the over pressure accumulator is the cause of a steady decline in pressure during a series of tests, making the determination of the condition less accurate. The combined error in σ is therefore not expected to lie below 10%. Since the focus is on the acoustic footprint only this is acceptable.

RESULTS: SINGLE BUBBLE IMPACT

A bubble in an unbounded flow collapses symmetrically at first, however, small surface perturbations or deviations in the assumed symmetry will result in a local acceleration of the bubble surface (micro jet formation). Lauterborn et.al.[4,5] showed for any bubble three times its dimensionless distance from a wall (γ=distance/bubble radius) that no strong micro jets are formed: the collapsing surface opposite of the forming micro jet also continues to accelerate unimpaired towards the jet and can thus also attain a high speed; this surface will impact and hinder the formation of a strong micro jet. For 1<γ<2 the micro jet is directed at the wall. The velocity of the bubble interface closest to the wall is sufficiently retarded to allow for a strong micro jet to form. For γ<1 the micro jet is formed but due to bubble migration towards the wall the micro-jet impinges on the wall. The collapse of a bubble in direct contact with the wall is thought to be the main cause for erosion.

In this experiment a spark probe generates the bubbles and the above description of a bubble collapse is lost: the probe always presents the bubble with a surface to collapse upon (resulting in surface deterioration of the probe). It is therefore not unexpected that for γ>1 the behavior of the bubble is consistent with a bubble collapse on the probe itself and the flow noise signal will remain constant. As the bubble will either break up on the probe or on the impact rod, the remaining structure consists of small bubbles with that rebounds could not be detected acoustically above 200 kHz.

Harmonic analysis shows that the probe detects signals up to 1,7 MHz, below the resonance frequency of 2Mhz specified by the

manufacturer. Several measured points per oscillation are present, peak values are never measured but always straddled, but a general trend is captured: the signal envelope is also reasonably symmetrical. As a result the measurement of a high peak is fortuitous and the measured peak intensities are indicative only.

The radius of the bubble is determined visually when the bubble has reached the end of its growth phase. Larger bubbles tend to migrate to the impact rod for smaller values of γ during the growth phase making an estimate of the maximum radius difficult. To estimate these effects, the growth and collapse time of the bubbles is compared with the collapse time from the Rayleigh equation:

$$R_{MAX} = \frac{1}{0.915}\sqrt{\frac{p - p_v}{\rho}}T_c \propto T_c \qquad (3)$$

As can be seen in fig. 2 some spread in the data is present, but a linear trend is discernable, both in the fluid as in the structure borne noise signals. The moment of growth and collapse is taken at the start of acoustic activity; peak-to-peak times show an even larger spread.

The signal measured in the fluid is presented in fig. 3. The peak at t=0 is the actual spark generation being electrical in nature interfering with the piezoelectric element. At Δt, a delay due to the traveling time of the pressure wave through the fluid, the bubble growth peak can be seen, including a reflection (The most probable cause is the translucent sheet that is placed a few centimeters behind the probe on which a strong light source is aimed for the cinematography, see fig. 1). The collapse peak and a few reflections can be seen some time later, at 4 ms. The bubble disintegrates into bubbly clouds that are visually rebounding, but the signal is very weak. A step in the trend is observed prior to the collapse, coinciding with the bubble wall impinging on the probe surface allowing for the probe to leak its remaining charge, sometimes large enough to spark another bubble. The time between the step in the trend and the bubble collapse peak is nearly constant in all tests (roughly Δt again), in other words, the location of the step shifts with the collapse of the bubble in time. Also, notice that prior to the highest collapse peak acoustic activity is measured. This can be caused by asymmetrical bubble collapse, micro jet impingement or the bubble wall striking the probe. This "pre-event" is consistently present in all fluid measurements.

Figure 4 shows a typical structure measurement. As can be seen, the damping of the signal is lower than in the fluid and a single peak value is less clearly present. Again the initial spark, delayed bubble creation and collapse can be identified in the signal. Identifying the various signals from the fluid signature in the structure signal is unclear as the reflections are overlapping.

As the distance to the hydrophone is kept constant, the intensity should be a function of R_{MAX} and γ only. As the collapse energy is related to the pressure squared which on its turn is related to the maximum radius, the measured peak intensity/R^2 is presented versus γ in fig. 5. Note that an energy estimate of a pressure transient is deliberately avoided as this value will be meaningless when compared to cloud collapse with a multitude of coinciding bubble collapses. The acoustic signal shows only a weak increase for a low γ, The behavior of the fluid signal is not unexpected as for γ>1,5 the bubbles collapse on the probe negating any relation with γ. More subtle techniques are needed to study the acoustic behavior of freely suspended bubble collapses. The structure signal clearly experiences a strong increase for
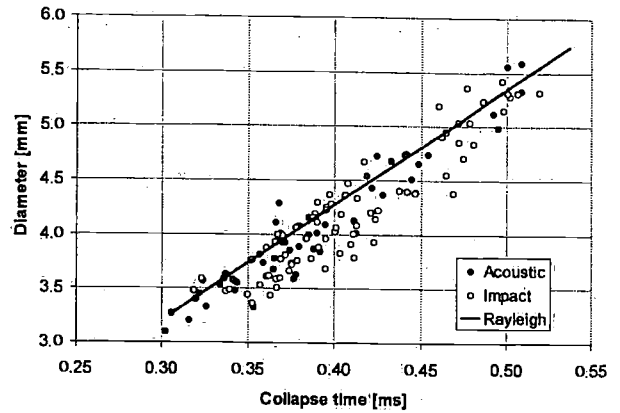

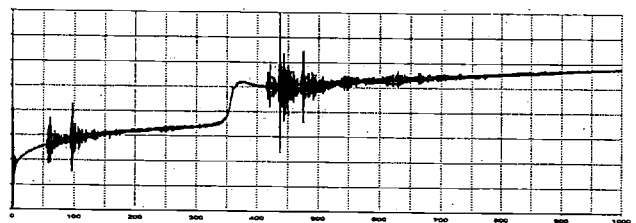Figure 2 Diameter versus collapse time for the single bubble setup

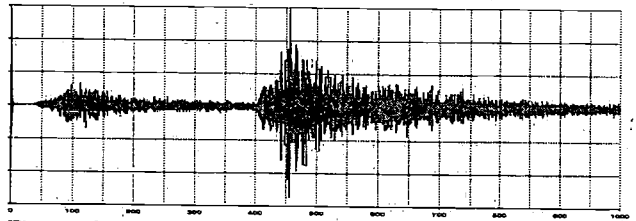Figure 3 (Unfiltered) Fluid signal of a typical bubble collapse. Total time 10 ms.

Figure 4 Structure signal of a typical bubble collapse. Total time 10 ms.
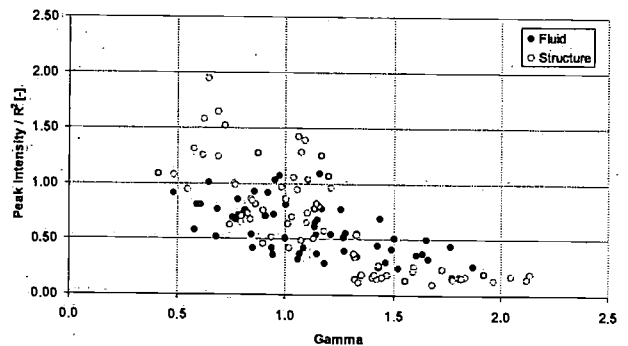

Figure 5 Peak intensity vs γ, fluid and structure signals

γ<1,3 in contrast to the fluid signal. A collapsing bubble near a surface leaves a clear highly frequent signal.

Figures 10 and 11 (page 5) present typical signals with frames grabbed from cinematography as a visual aid. The voluminous spark plug is visible at the left side of each frame, the impact object at the top. The largest part of the growth and collapse phase is silent.

RESULTS: SHEET IMPACT

The Naca foil is placed at an angle of attack of 10 degrees, see figs. 12-17 on page 6. For 2,4<σ<3,0 the sheet is thin and displays typical '2D' behavior, with local patches shedding from the main cavity with a length that remains constant. At σ=2.2 the cavity is thick enough for a re-entrant jet to cause structures on the same length scale as the sheet to break off. At σ=1,9, the sheet and cloud cavities approach the length of the foil itself. However, the collapsing structures are visibly some distance from the surface of the foil.

The acoustic signal measured is expectedly more complex than a single bubble collapse but reflects the single bubble characteristics; a multitude of impact signals can be identified (fig. 6). Reverberations and reflections are naturally more abundant than in the single bubble impact method. An FFT shows a wide band in the energy spectrum with a peak at 19,5 kHz. This peak frequency is independent on the pump tunnel rpm, flow velocity, angle of attack or σ, but does increase in magnitude for increased cavitation volumes and is dismissed as a natural frequency of some tunnel component.
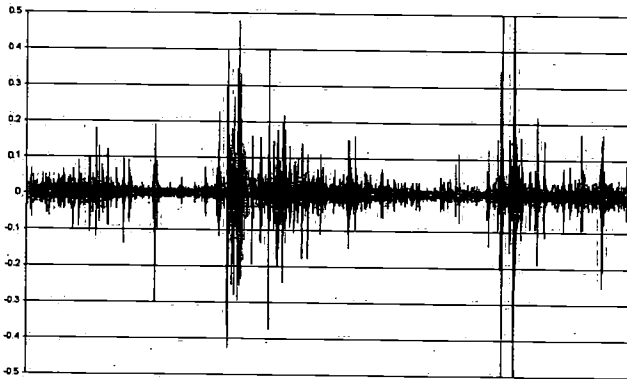

Figure 6 Fluid borne noise of collapsing sheet cavitation (20 ms)

As a first attempt at analyzing the signal, a recording with arbitrary length is taken. The signal level is divided into a number of contiguous bands. The number of occurrences per bandwidth are counted constituting a probability distribution of an exponentially decreasing type. This exercise, plotted in fig. 7, shows the signals to be repeatable and to be a clear function of σ.
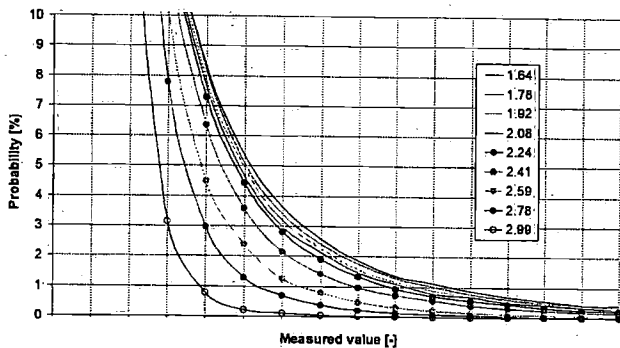

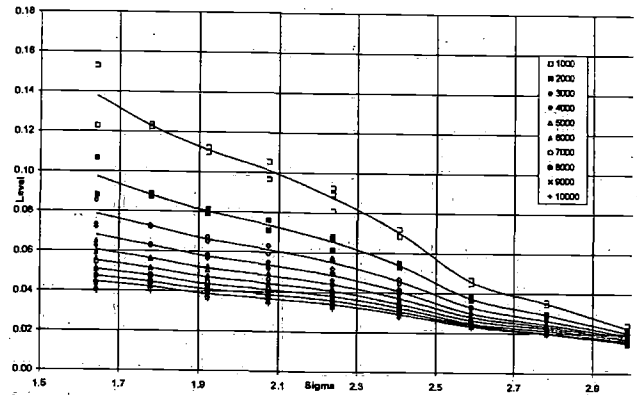Figure 7 Probability distribution for acoustic signal levels at various σ
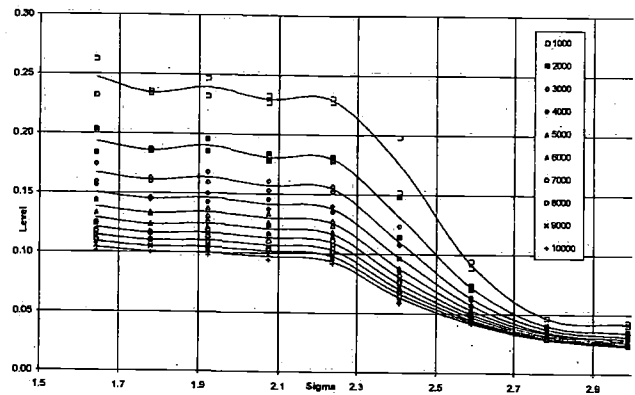

Figure 8 Fluid signal peakogram

Figure 9 Structure signal peakogram

One can take the cumulative distribution and estimate the level at which a threshold value is exceeded a certain number of times. An example is given in fig. 8 with a plot of these thresholds versus σ, termed the peakogram. For a low threshold the statistical scatter causes some variation, decreasing for higher thresholds. The measured level and number of times the threshold is exceeded is chosen arbitrarily.

The structure signal follows a trend similar to the single bubble impact method. As expected, the signal is more clouded by reflections and reverberations. Many high peaks can be seen throughout the measurement, independent of the shedding frequency. As the sensor is much closer to the source, and the damping of the material is low, the signal is much stronger than the fluid signal. From the single bubble impact test it is already known that a simple pressure wave can result in a complex response.

Comparing this peakogram of the signal from the fluid with the peakogram (fig. 9) from the sensor in the foil itself, a striking difference in trends can be seen. Although the acoustic activity is clearly increasing for a decreasing σ, the structure borne noise remains of equal intensity for σ<2,2. The observations indicate that the collapse of the main cavity structure migrates from the foil surface for decreasing σ, translating into a decrease in the ratio of structure versus fluid borne noise visible in the diagrams.

CONCLUSIONS

The collapse of a single bubble of 3-5 mm leaves a short acoustic foot print above 200 kHz, far higher than background or other flow noise . This signal can be picked up by transducers in a structure if this collapse is near ($\gamma<1,5$). For $\gamma>1,5$ the bubble collapses on the spark probe used to generate the bubble in this experiment. For low γ, the structure borne noise intensity increases quickly. The fact that both fluid and structure noise increase with decreasing distance to the surface indicates that is may be possible to detect surface erosion both from the fluid and the structure borne noise. This might be further explored, as fluid borne noise is easier to measure.

The experiments with the sheet cavitation in the small water tunnel indicate that both fluid and structure borne noise above 200 kHz resembles the agglomerated signal of a multitude of single bubble collapses. The intensity of fluid born noise increases with the observed cavitation patterns, but structure born noise reduces in strength when the imploding cavities are further from the surface. The signal shows statistical repeatability over a number of shedding periods. The single bubble experiments indicated that the implosion strength is increased with a deceasing distance to the wall. This relation is less clear in the foil experiments, since the decreasing cavitation number changes both the location and strength of the implosion. The foil experiments show a stronger difference between fluid and structure born noise attributed not only attributed to the distance between the implosion and the surface, but also to acoustic screening of additional cavitation between the surface and the implosion at lower cavitation numbers. The strength of the implosion indicates its strength, the structure borne noise seems to be a better indicator for the risk of erosion; it remains uncertain if the risk can be quantified with calibrated sensors at this time.

ACKNOWLEDGEMENTS

REFERENCES

[1]Escaler, X; Avellan, F; Egusquiza, E, 2001, "Cavitation erosion prediction from inferred forces using material resistance data", Cav2001, 4th International Symposium on Cavitation, A3.005

[2]Lorhberg, H; Stoffel, B, 2001 "Measurement of cavitation erosive aggressiveness by means of structure born noise", Cav2001, 4th International Symposium on Cavitation, A3:003

[3]Ohl, C D; Philipp, A; Lauterborn, W, 1995, "Cavitation bubble collapse studied at 20 million frames per second", An. Physik 4, pp 26-34

[4]Vogel, A; Lauterborn, W; Timm, R, 1989, "Optical and acoustic investigations of the dynamics of laser-produced cavitation bubbles near a solid wall", J. Fluid Mechanics, 206 pp 299-338

[5]Philipp, A; Lauterborn, W, 1998, "Cavitation erosion by single laser-produced bubbles", J. of Fluid Mechanics, 361, pp 75-116
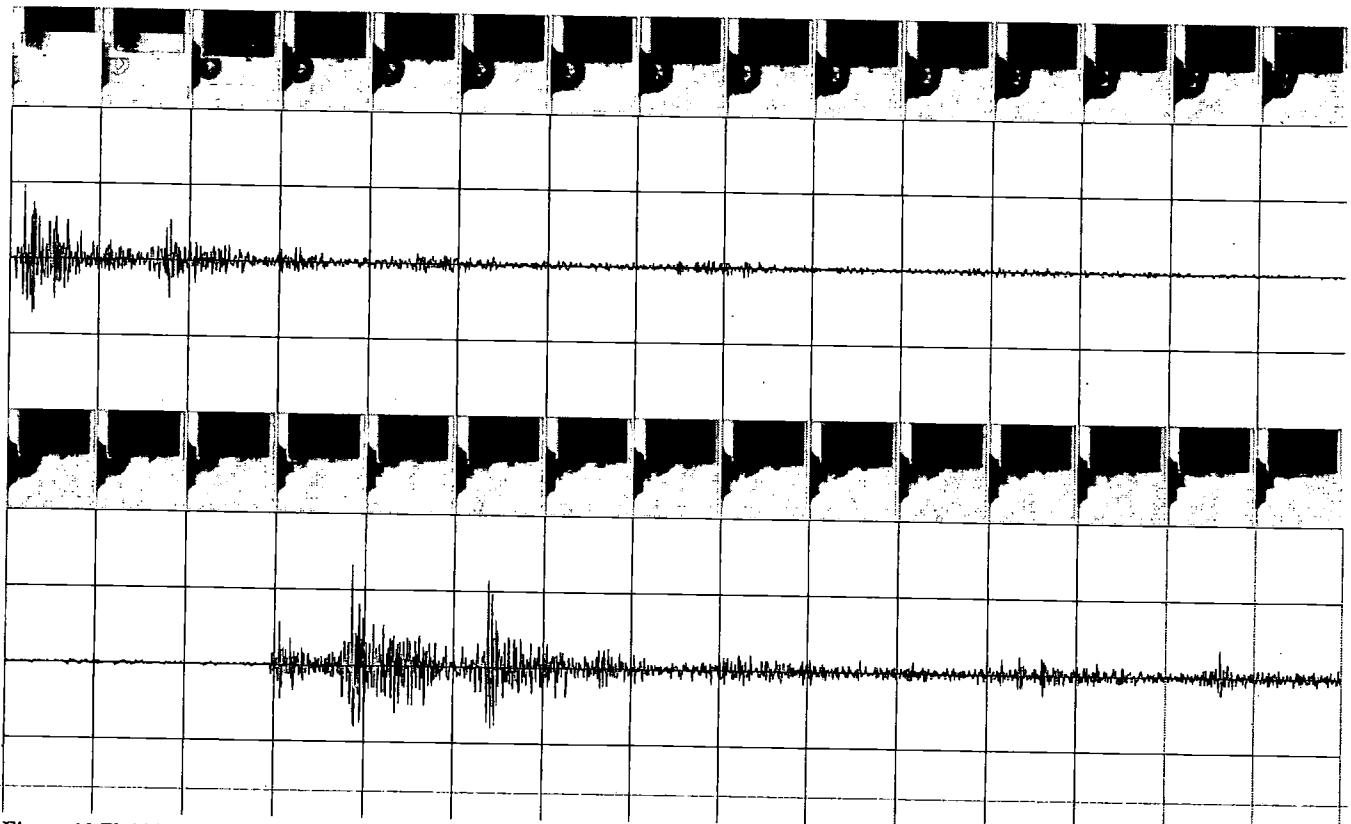
Figure 10 Fluid borne noise with frames from cinematography. Fluid signal shifted 55,7 µs to correct for the traveling time of a sound wave to the hydrophone

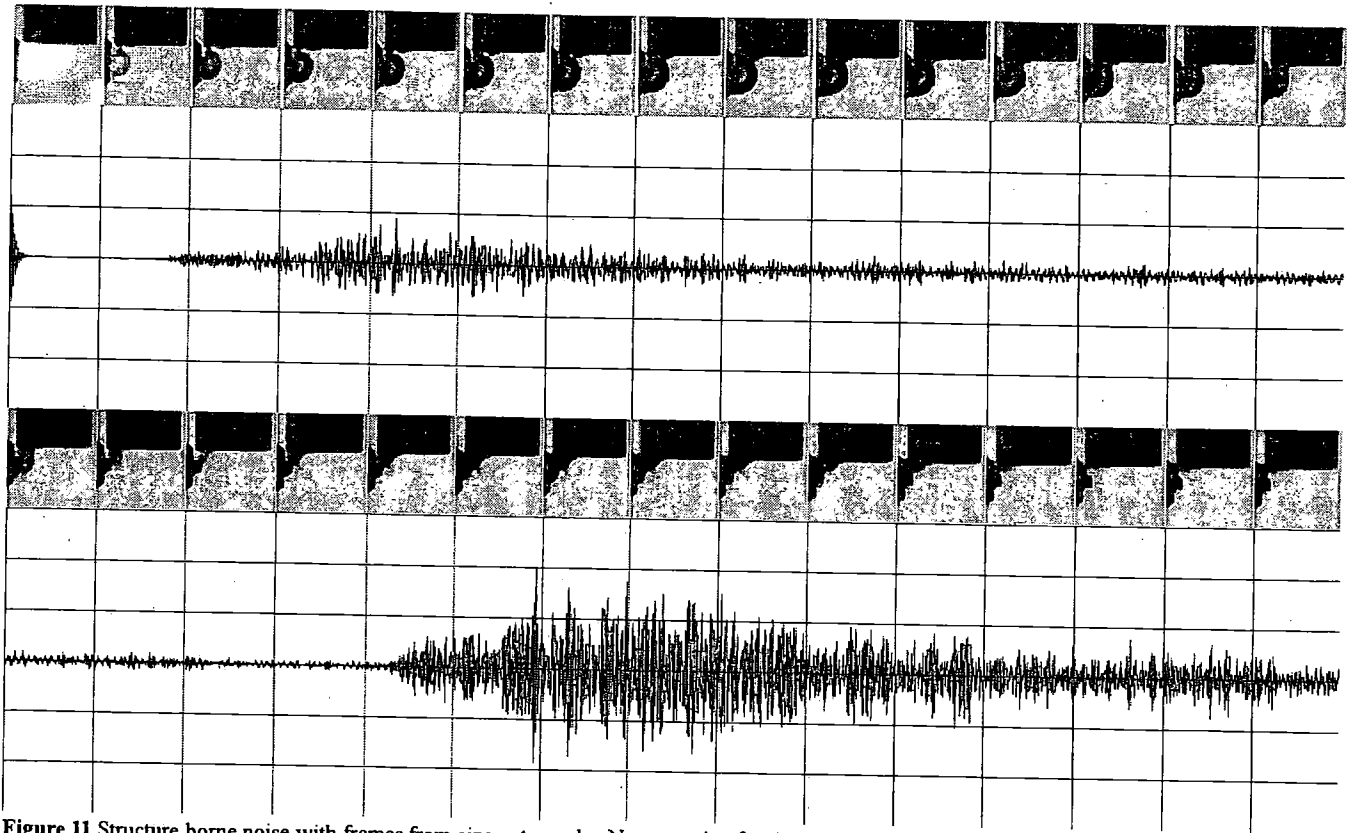**Figure 11** Structure borne noise with frames from cinematography. No correction for time is made.
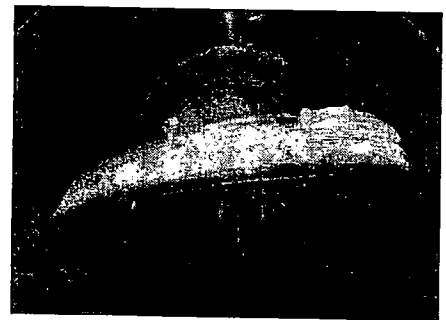

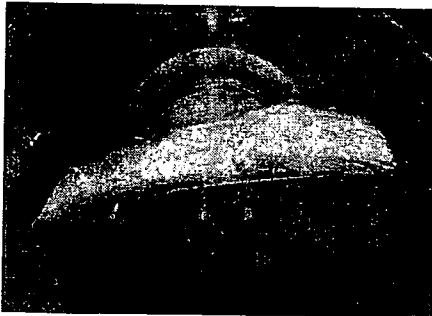**Figure 12** σ=3,0

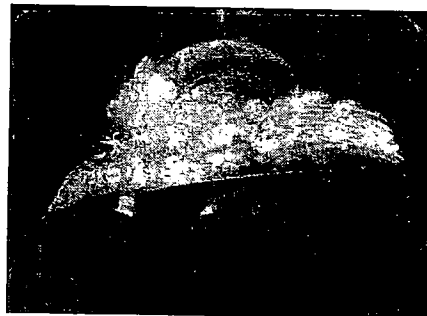**Figure 13** σ=2,6
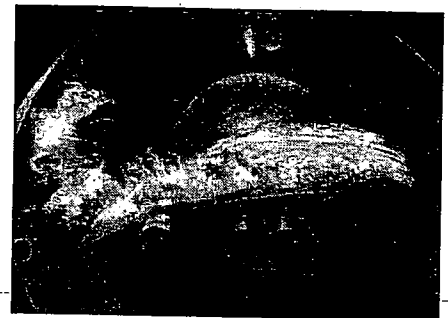

Figure 14 σ=2,4

Figure 15 σ=2,2

Figure 16 σ=1,9

Figure 17 σ=1,8

Figures 12 to 17 show a Naca0018-45 hydrofoil at various values of σ. Full sheet roll-up commences for σ<2,2.